Nanoscale

Accepted Manuscript

This article can be cited before page numbers have been issued, to do this please use: J. Bian, X. Xing, S. Zhou, Z. Man, Z. Lu and W. Zhang, *Nanoscale*, 2019, DOI: 10.1039/C9NR00455F.

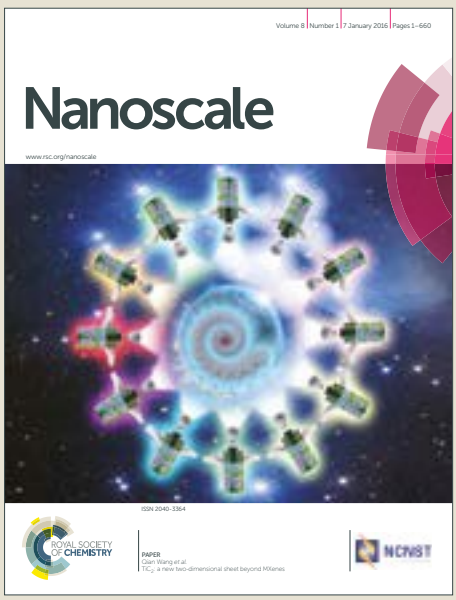

ROYAL SOCIETY OF CHEMISTRY

rsc.li/nanoscale

View Article Online
DOI: 10.1039/C9NR00455F

Nanoscale

COMMUNICATION

Patterned plasmonic gradient for high-precision biosensing using smartphone reader

Received 00th January 20xx,
Accepted 00th January 20xx

DOI: 10.1039/x0xx00000x

www.rsc.org/

Jie Bian, Xing Xing, Shuang Zhou, Zaiqin Man, Zhenda Lu* and Weihua Zhang*

Smartphone-compatible biosensors are believed to be one of the key techniques for improving the quality of diagnosis in remote areas. However, to date, few smartphone-compatible biosensors can reach the specifications of their conventional counterparts due to the limitations of consumer-grade detectors carried by phones. To circumvent this issue, we reported a metasurface-inspired bio-sensor, patterned plasmonic gradient (PPG), which transduces local index information into 2D patterns. By harnessing the powerful imaging and computation capability of modern smartphones, the PPG is sensitive enough to detect tiny refractive index changes induced by a submonolayer of molecules with high precision (Δn < 0.001) in a large dynamic range. It allows us to monitor the conjugation process between biotin and a trace amount of streptavidin (15 nM, 20 μL) in real-time. With the high sensitivity and accuracy, the PPG provides a high performance bio-sensing solution for the places where professional equipment is inaccessible.

Today, with the high penetration of smartphones in our daily life, the demand for smartphone-compatible diagnostic tools arises rapidly[1-8]. Along this trend, an interesting possibility is to shrink the surface-plasmon resonator (SPR) sensor, a widely used molecular diagnostic tool, into a small chip-like device which can be directly read and analyzed by a smartphone[9, 10]. However, this is challenging due to the design of current SPRs, which are either thin films[11] or periodic arrays of nanostructures (i.e. nanoparticles[12, 13], nanoholes[14-16] and nanocavities[17, 18]). To achieve high accuracy, one needs to measure either the spectral or angular information of the SPR sensors, and this often requires bulky and sophisticated instruments[11, 19]. Meanwhile, with the emergence of metasurface, nonperiodic nanostructures become popular[20-22]. This leads to the new opportunity for designing SPR systems with unconventional readout methods. Inspired by this, here we introduce a nonperiodic plasmonic sensor, the patterned plasmonic gradient (PPG). It can transduce a minute change of its local environment into the drifts of 2D optical patterns, which can be directly read and analyzed using a smartphone-based reader. This strategy is particularly powerful today as the performance of phone-carried camera (resolution of the imaging sensor and quality of the lens) and phone-based microscopes has been improved dramatically over the last few years.[23, 24]

The central idea of the PPG technique is to convert spectral information into spatial information using a continuously varied plasmonic nanoantenna array (i.e. plasmonic gradient), in which the resonance wavelength of the antennas, $\lambda_{res}(x, y, n)$, is a function of space (x, y) and the refractive index of its surrounding medium, n.[25] The total differential of resonance wavelength can then be written as

$$\Delta\lambda_{res} = \frac{\partial\lambda_{res}}{\partial x}\Delta x + \frac{\partial\lambda_{res}}{\partial y}\Delta y + \frac{\partial\lambda_{res}}{\partial n}\Delta n \quad (1)$$

In conventional SPRs, the resonance is spatially independent (i.e. $\partial\lambda_{res}/\partial x = \partial\lambda_{res}/\partial y = 0$), and the index change is reflected in the resonance wavelength change, $\Delta\lambda_{res}$ of the nano-antennas. In this work, $\partial\lambda_{res}/\partial x \neq 0$, $\partial\lambda_{res}/\partial y \neq 0$, and therefore environmental index changes will be reflected on the contour lines of resonance wavelength of the PPG structure via relation

$$\frac{\partial\lambda_{res}}{\partial n}\Delta n = -\frac{\partial\lambda_{res}}{\partial x}\Delta x - \frac{\partial\lambda_{res}}{\partial y}\Delta y \quad (2)$$

With this design, Δn can be explicitly derived from the spatial variations of resonance contour line (i.e., Δx and Δy) which can be directly captured with the camera of a smartphone.

College of Engineering and Applied Sciences, National Laboratory of Solid State Microstructures, Collaborative Innovation Center of Advanced Microstructures and Jiangsu Key Laboratory of Artificial Functional Materials, MOE Key Laboratory of Intelligent Optical Sensing and Manipulation, Nanjing University, Nanjing, 210093, P.R. China. E-mail: luzhenda@nju.edu.cn; zwh@nju.edu.cn

† Footnotes relating to the title and/or authors should appear here.
Electronic Supplementary Information (ESI) available: [Theoretical considerations and the Refractive index of sucrose solution]. See DOI: 10.1039/x0xx00000x

View Article Online
DOI: 10.1039/C9NR00455F

To demonstrate the PPG technique, we take a simple case, the square patterned plasmonic gradient (SPPG), as an example. As illustrated in Figure 1, the SPPG is a 2D array of Au nanorods with a pitch size of 300 nm and the length of Au nanorods increasing linearly from 80 nm at the center to 200 nm at the peripheral of the array. Because the resonance wavelength of a plasmonic nanorod is linearly dependent on its aspect ratio[26, 27], the SPPG exhibits a square-shaped color gradient correspondingly, as depicted in Figure 1b.

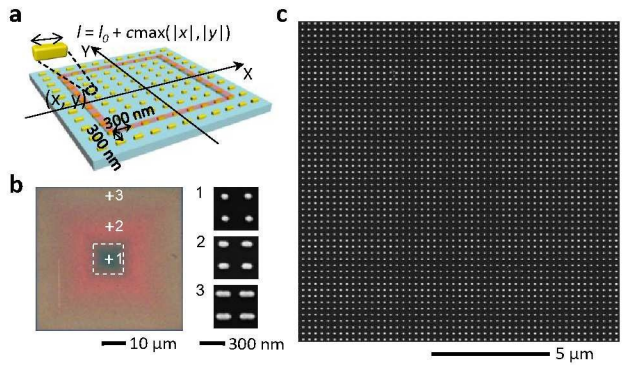

Fig. 1 Design of the SPPG sensor. (a) Geometrical layout of the SPPG structure. The length of Au nanorods increases linearly from the center to the periphery. (b) Optical image of a typical SPPG sample. The insets are the SEM images at the positions labeled in the optical image. (c) The SEM images of the central part of the SPPG sample labeled by the dashed line square in (b).

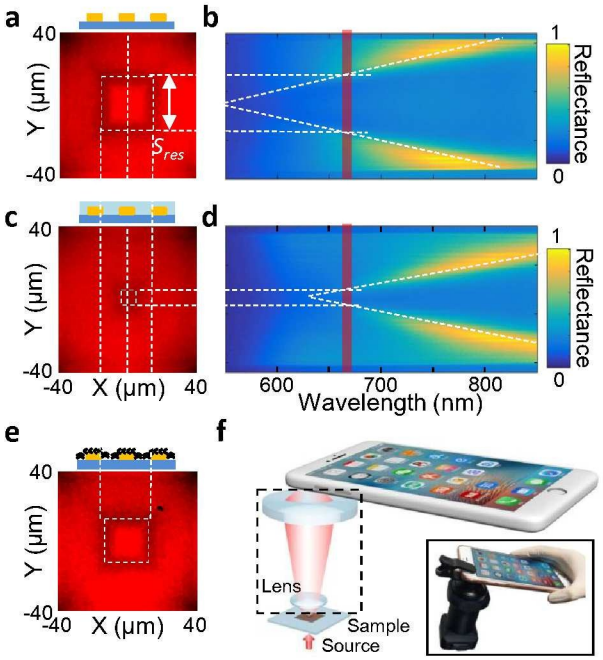

Fig. 2 Pattern-based index sensing experiment. (a), (c) and (e) is the transmission image of a SPPG sensor in air, ethylene glycol (n = 1.3933) and with a submonolayer of HS-PEG2000-COOH, respectively. The results were recorded by a smartphone reader, and size changes of resonance ring were observed. (b) and (d) is the map of refraction spectra along the symmetrical axis labeled by the dashed line in (a) and (c), respectively. (f) The schematic drawing of the smartphone-based microscope reader. The inset shows the photo of the reader by 3D-printing.

In experiment, the resonance contour line at wavelength, λ_{res}, can be directly visualized by illuminating sample with monochromic light at λ_{res} (Figure 2a). As aforementioned, the resonance wavelength of the SPPG increases linearly from the center to periphery. At positions where nanorods resonantly match with the excitation wavelength transmission reaches the minimum, and consequently a dark ring (i.e. iso-resonance ring) forms. Here, we performed the measurements using a low-cost 3D-printed microscope and iPhone X with transmission mode (unpolarized illumination by a LED, 660 nm, FWHM = 6 nm).

Thanks to the high spectral sensitivity of plasmonic nanorods, the SPPG structure enjoys high sensitivity. To demonstrate this point, we mapped the reflection spectra along the central axis of the SPPG before and after it was immersed in ethylene glycol (n =1.3933). As illustrated in Figure 2b and 2d, resonance wavelength redshifts by more than 100 nm, and consequently, the resonant ring shrinks into a small spot at the centre of the SPPG.

Equipped with the high sensitivity, SPPG is capable of detecting even a submonolayer of molecules. To illustrate this, we functionalized the sample SPPG with a submonolayer of organic molecules (HS-PEG2000-COOH). Figure 2d shows the iso-resonant ring of the same SPPG sample measured by the smartphone reader, and an evident size change (8.06%) of the iso-resonance ring was observed. This provides a direct proof for the high sensitivity of SPPG.

In addition to the high sensitivity, the SPPG can be utilized as a quantitative analysis tool since the dimension of square resonance ring of a SPPG, S_{res}, follows a simple inverse proportion law with the environmental refractive index,. This $S_{res} \propto 1/n$ law can be derived from the spatial dispersion relation of the SPPG sensor. It is known that the resonance wavelength, λ_{res}, follow a simple relation:

$$\lambda_{res} = \lambda_p \sqrt{\varepsilon_b + aR^2 n^2} \quad (3)$$

Here ε_b and a are constants, $R = l/w$, the width of the nanorods w is fixed, and the length of nanorods $l(x, y) = 80\ \text{nm} + c_{\max}(|x|, |y|)$ with $c = 1$. From equation (1) and (3), we can obtain an explicit relation between S_{res} and n (details can be found in the supporting information):

$$S_{res} = \frac{\lambda_{res} w S_{SPPG}}{\lambda_p \sqrt{a} \Delta l n} - \frac{l_0 S_{SPPG}}{\Delta l} \quad (4)$$

where S_{SPPG}, l_0 and Δl is the size of the SPPG, the length of the shortest nanorod and the length difference between the longest and shortest nanorods, respectively.

In practice, we measure the normalized size S_{res}/S_{SPPG} instead of the absolute size S_{res} in order to reduce the readout errors of the system. The inaccuracy of the absolute value of S_{res} induced by the instability of optical imaging system can be

View Article Online
DOI: 10.1039/C9NR00455F

effectively calibrated in the normalization process. This self-calibration capability is important for field experiments, where stable measurement environments cannot be guaranteed.

We experimentally examined the linear dependence of S_{res}/S_{SPPG} on $1/n$ by measuring the $A_{res} = S_{res}^2$ at 780 nm with the SPPG sample immersed in sucrose solution with different concentrations (0 – 60 wt %, and the refractive index varies from 1.334 to 1.447[28]). In this measurement, illumination at 780 nm was used because, in air, the corresponding resonant ring is close to the edge of the sensor and this will lead to a large dynamic range for measurements.

Figure 3 shows the experimental result. A near perfect linear relation was found between S_{res} and $1/n$, as predicted by equation (4). The correlation coefficient was 0.9991, and the standard deviation was 9.1E-4. In other words, the accuracy of SPPG sensor is better than 1E-3, comparable with the best results of conventional SPR equipment without additional signal amplifications[29, 30].

The inverse proportion law holds as far as the iso-resonant ring is within the SPPG sample, and this leads to a large dynamic range for SPPG structures. To illustrate this point, we experimentally varied the refractive index of the surrounding medium of a SPPG sample from 1.000 to 1.738 with different matrices (air, deionized water, ethylene glycol, 4-methyl-2-pentanone, anisole and methylene diiodide), and the iso-resonant line moved from the edge of SPPG to the center correspondingly, as shown in Figure 3b. Similar to the case of small index changes, near-perfect linear dependence of S_{res}/S_{SPPG} on $1/n$ was observed, as shown in the inset of Figure 3a. The coefficient was 0.9922 (inset of Figure3a).

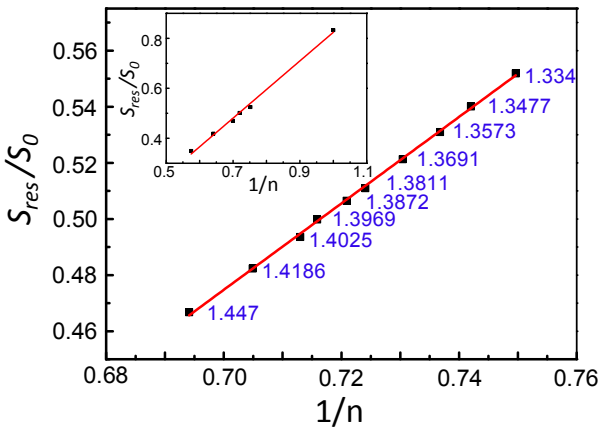

Fig. 3 Index-dependent resonant ring size. Size of the resonant ring of a SPPG observed in sucrose solutions with the concentrations varied from 0% to 60% (refractive index: 1.334 to 1.447). The inset is the measured S_{res}/S_{SPPG} - 1/n curve in a broader index range (1.000 to 1.738).

With the high sensitivity, SPPG structures can be applied in many important biochemical measurements, particularly the real-time measurement of chemical conjugation processes. To demonstrate this, we measured the adsorption process of streptavidin, one of the most widely used model systems in biosensing. In the measurement, the SPPG was first functionalized using the standard procedure in SPR experiments, and then 20 µL streptavidin solution (15 nM) was added. We monitored the resonance ring of the SPPG sensor under 780 nm illumination, calculated the size of the area enclosed by the iso-resonant ring using a homemade program, and plotted the size of the resonance ring as a function of time. Since the test was longer than 10 minutes, the experiment was performed using an inverted microscope (Olympus, IX-73) instead of the smartphone reader. Here, bright iso-resonance rings were observed since the reflection mode was used instead of transmission.

Figure 4 shows a typical result. The adsorption of streptavidin molecules on the SPPG alters the local refractive index and consequently shifts the resonance ring slightly, causing the change of S_{res}. The kinetic behavior of the S_{res}/S_{SPPG} vs.t curve is comparable to the results in SPR experiment[31], showing a rapid adsorption rate at the beginning and then a graduate saturation. Here, the concentration of the streptavidin is 15 nM, which is comparable to previously reported value in SPR measurements without additional signal amplification[29, 30].

Here, since the signal to noise ratio in Fig. 4a is high (approximately 20), the LoD of Streptavidin is expected to be at ~1 nM (100 ng/mL) level. This is comparable with the smartphone SPR systems based on angular spectrum measurements[32, 33], and considerable better than the fiber-based plasmonic sensor[34], as well as the plasmonic hole-array sensor[8].

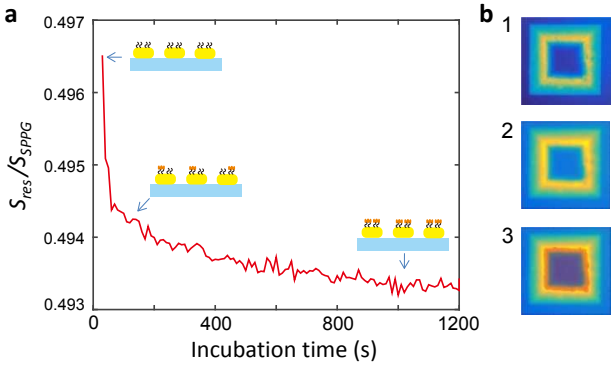

Fig. 4 Realtime measurement of the adsorption process of Streptavidin. (a) Size the resonance ring as a function incubation time. (b) Major data processing steps, namely, 1 the raw data, 2 data after smoothing, and 3 result after the iso-resonant ring search and filling.

It is worth noting that due to the random adsorption of protein molecules in assay experiments the resonance shifts of the Au nanorods in SPPG can be in homogeneous at the sub-micrometer scale. Nevertheless, in the micrometer scale, the area average adsorption is homogeneous, and it is therefore crucial to smooth the data in order to improve the accuracy. In this work, this job is done by a homemade data analysis program. It smooths the data to remove random noises, finds the resonant rings, and calculates the size of the rings by filling it, as demonstrated in Figure 4b. Results show that the signal-

View Article Online
DOI: 10.1039/C9NR00455F

to-noise ratio can be improved by more than one order of magnitude with the data smoothing step. In addition, the smoothing step also makes the device insensitive to defects, which sometimes occur in large array structures.

One unique feature of the SPPG sensor is that its sensitivity is not a fixed value and can be further improved. To elucidate this point, we define the sensitivity of the system as $\eta = dS_{res,i}/dn$, where $S_{res,i}$ is the dimension of resonant square on the image plane of the reader. From equation (4), we have

$$\eta = \frac{dS_{res,i}}{dn} = \frac{\lambda_{res} w S_{SPPG}}{\lambda_p \sqrt{a} \Delta ln^2} M \quad (5).$$

It is evident that sensitivity of a SPPG sensor is proportional to its size, S_{SPPG}, and the magnification of the reader, M, and therefore can be improved simply by increasing sample size or the magnification of the reader. This is fundamentally different from the conventional SPR and LSPR sensors, in which the sensitivity is limited by the material and shape of the sensor.[35]

The limit of detection (LoD) of SPPG can also be derived. In this work, size $S_{res,i}$ is determined by numerical fitting. According to the statistical theory, the uncertainty is determined by the full width half maximum of the resonance ring (FWHMi) and the counts, N, measured by the detector:

$$\delta S_{res,i} \propto \frac{FWHM_i}{\sqrt{N}} \quad (6).$$

The LoD of the refractive index change, δn, can then be derived as (details can be found in the supporting information),

$$\delta n \propto \frac{\sqrt{a_{pix}}}{M^2 S_{SPPG}{}^2} \quad (7).$$

Here, a_{pix} is the pixel size of the camera.

In equation 5 and 7, we learn that the sensitivity and LoD of SPPG can be further improved by increasing the size of the sensor and magnification of the reader. However, in practice, it is not feasible to further improve the magnification since expensive lens system will be needed, and therefore, increase of the sensor size becomes important. In this work, the SPPG chips were fabricated by e-beam lithography, and because of the high cost and slow fabrication speed, it is challenge to further increase the sensor size. Fortunately, new techniques were reported recently for fabricating large area gradient nanostructures, such as partial evaporation on rotating substrate[36], mechanical stretching[37], and Moire pattern based lithography[38]. We believe that these new fabrication techniques can lead to significant improvement of the PPG sensors. Moreover, with low cost duplication techniques, e.g. nanoimprint lithography[39], the fabrication cost of SPPG can be significantly reduced, and this is crucial for future applications of SPPG.

Conclusions

In summary, we developed a new type of metasurface inspired bio-sensor, the SPPG, which encodes the spectral information into spatial information using a gradient design and can therefore be directly read by a smartphone camera. Thanks to the powerful imaging sensor and computation capacity of modern smartphones, SPPG sensor can measure tiny index changes by a submonolayer of molecules in a quantitative fashion. This allows us to monitor the conjugation process of a trace amount of analyte in real time. The results show that the performance of the SPPG is comparable with commercial tabletop SPR systems. Here, we would like to emphasize that the SPPG sensor is only the first attempt of spatially encoded plasmonic sensors, and there are plenty of room for further improvement. We believe that, with the high performance, robustness and potential low-cost, the pattern-based plasmonic sensors will lead to many new possibilities, including high quality diagnosis in rural area, fast water and food safety inspection and other field applications.

Experimental

Fabrication of SPPG structure.

SPPG samples in this work were fabricated by electron-beam lithography on glass substrates. First, negative resist (AR-N 7520, Allresist) was spun on an Au (30 nm) coated cover glass, followed by 1 min baking at 85 ℃. Then, the sample was patterned with electron beams at 30 keV using a scanning electron microscope (Ultra 55, Zeiss) with a nanopattern generation system (NPGS), and subsequently developed to form gradient array patterns using developers (AR300-47, Allresist) at 21 ℃ for 50 s. Finally, SPPGs were formed by transferring the gradient patterns to the Au layer using argon plasma etching.

Smartphone reader.

The readout gadget is small (1" × 1" × 3" in size) and simple, consisting an adjustable sample holder, magnification lenses and a flat LED for illumination. To achieve homogeneous illumination, a diffuser was placed between the sample and LED. It is worth mentioning that although a 80X microscope objective lens is used in current gadget and this can actually be replaced by a low-cost smartphone camera lens[24]. It will lead to a compact design, as well as a significant reduction of cost. To retrieve the value of S_{res}/S_{SPPG} from a picture, codes were written on both Android system (i.e., APP for smartphone) and Windows system (for PC). It allows us to calculate the ring size directly from pictures of the sample.

Spectral mapping of SPPGs and reflection measurement.

The reflection spectra of SPPGs were mapped using a microscopic spectrometer which consists of an inverted microscope (IX 73, Olympus) and an imaging spectrometer (SR303, Andor) with a CCD camera (iDus 401, Andor). In experiments, the spectra along the symmetric axis of SPPGs were collected by carefully aligning the axis with the entrance

View Article Online
DOI: 10.1039/C9NR00455F

axis of the imaging spectrometer.[40] Since the reflection mode was used, bright resonant isolines were observed instead of dark ones in the transmission mode by the smartphone reader.

Immobilization and detection of streptavidin.

We first functionalized the SPPG sample with carboxylic group by incubating it in 10 mM MUA ethanol solution over night and subsequently in EDC/NHS solution (400 mM of EDC and 100 mM of NHS dissolved in 10 mM of PBS buffer, pH 7.0) for 30 min. The sample was then immersed in biotin-PEG2-amine solution (20 mM in PBS buffer) for 30 min to form covalent binding between carboxylic and amine groups. After PBS rinsing, Ethanolamine PBS solution (50 mM) was added and the sample was incubated for 30 min to seal the remaining unreacted carboxylic group followed by the final thorough rinsing. After that, the SPPG substrate mounted on the optical microscope, ready for recording the resonant rings. Streptavidin PBS solution (20 µL, 1.0 µg/mL) was dropped onto the substrate to allow adsorption on the Au nanorods via the specific biotin-streptavidin reaction. The whole adsorption process was recorded by the camera.

Conflicts of interest

There are no conflicts to declare.

Acknowledgements

This study was supported by grants from the National Key Technologies R&D Program of China (No. 2016YFA0201104), National Basic Research Program of China (No. 2015CB659400), National Natural Science Foundation of China (No. 11574142, 11621091, and 21601083). We thank Prof. Ying Liu for discussions.

References

1. J. C. Contreras-Naranjo, Q. Wei and A. Ozcan, *IEEE J. Sel. Top. Quant.*, 2016, **22**, 1-1.
2. D. J. You, T. S. Park and J.-Y. Yoon, *Biosensors & Bioelectronics*, 2013, **40**, 180-185.
3. D. Quesada-Gonzalez and A. Merkoci, *Biosensors & Bioelectronics*, 2017, **92**, 549-562.
4. S. Dutta, G. P. Saikia, D. J. Sarma, K. Gupta, P. Das and P. Nath, *J.Biophotonics*, 2017, **10**, 623-633.
5. J. Hu, X. Cui, Y. Gong, X. Xu, B. Gao, T. Wen, T. J. Lu and F. Xu, *Biotechnol. Adv.*, 2016, **34**, 305-320.
6. K. A. Oliveira, D. Damasceno, C. R. de Oliveira, L. A. da Silveira, A. E. de Oliveira and W. K. T. Coltro, *Anal.Methods*, 2016, **8**, 6506-6511.
7. L. Zhang, W. Yang, Y. Yang, H. Liu and Z. Gu, *Analyst*, 2015, **140**, 7399-7406.
8. X. Wang, T.-W. Chang, G. Lin, M. R. Gartia and G. L. Liu, *Anal. Chem.*, 2017, **89**, 611-615.
9. Q. Fu, Z. Wu, F. Xu, X. Li, C. Yao, M. Xu, L. Sheng, S. Yu and Y. Tang, *Lab Chip*, 2016, **16**, 1927-1933.
10. T. Yu and Q. Wei, *Nano Res.*, 2018, **11**, 5439-5473.
11. B. Liedberg, C. Nylander and I. Lundstrom, *Biosensors & Bioelectronics*, 1995, **10**, R1-R9.
12. A. J. Haes and R. P. Van Duyne, *J. Am. Chem. Soc.*, 2002, **124**, 10596-10604.
13. J. C. Riboh, A. J. Haes, A. D. McFarland, C. R. Yonzon and R. P. Van Duyne, *J. Phys. Chem. B*, 2003, **107**, 1772-1780.
14. A. G. Brolo, R. Gordon, B. Leathem and K. L. Kavanagh, *Langmuir*, 2004, **20**, 4813-4815.
15. T. W. Ebbesen, H. J. Lezec, H. F. Ghaemi, T. Thio and P. A. Wolff, *Nature*, 1998, **391**, 667-669.
16. R. Gordon, D. Sinton, K. L. Kavanagh and A. G. Brolo, *Acc. Chem. Res.*, 2008, **41**, 1049-1057.
17. D. Chanda, K. Shigeta, T. Tu, E. Lui, A. Mihi, M. Schulmerich, P. V. Braun, R. Bhargava and J. A. Rogers, *Nat.Commun.*, 2011, **2**, 479.
18. Y. Shen, J. Zhou, T. Liu, Y. Tao, R. Jiang, M. Liu, G. Xiao, J. Zhu, Z.-K. Zhou, X. Wang, C. Jin and J. Wang, *Nat.Commun.*, 2013, **4**, 2381.
19. J. N. Anker, W. P. Hall, O. Lyandres, N. C. Shah, J. Zhao and R. P. Van Duyne, *Nat.Mater.*, 2008, **7**, 442-453.
20. N. Yu and F. Capasso, *Nature Materials*, 2014, **13**, 139-150.
21. N. Yu, P. Genevet, M. A. Kats, F. Aieta, J.-P. Tetienne, F. Capasso and Z. Gaburro, *Science*, 2011, **334**, 333-337.
22. G. Quaranta, G. Basset, O. J. F. Martin and B. Gallinet, *ACS Photonics*, 2017, **4**, 1060-1066.
23. X. Meng, H. Huang, K. Yan, X. Tian, W. Yu, H. Cui, Y. Kong, L. Xue, C. Liu and S. Wang, *Lab chip*, 2016, **17**, 104-109.
24. N. A. Switz, M. V. D'Ambrosio and D. A. Fletcher, *Plos One*, 2014, **9**, e95330.
25. K. M. Mayer and J. H. Hafner, *Chem. Rev.*, 2011, **111**, 3828-3857.
26. K.-S. Lee and M. A. El-Sayed, *J. Phys. Chem. B*, 2006, **110**, 19220-19225.
27. L. Novotny, *Phys. Rev. Lett.*, 2007, **98**, 266802.
28. W. Zhou, S. Luo, C. Wang and X. Zhang, *Journal of Xingyi Normal University for Nationalities*, 2013, **5**, 119-121.
29. H. J. Lee, A. W. Wark and R. M. Corn, *Analyst*, 2008, **133**, 975-983.
30. Y. Liu and Q. Cheng, *Anal. Chem.*, 2012, **84**, 3179-3186.
31. Y. Liu, P. Liao, Q. Cheng and R. J. Hooley, *J. Am. Chem. Soc.*, 2010, **132**, 10383-10390.
32. P. Preechaburana, M. C. Gonzalez, A. Suska and D. Filippini, *Angew. Chem. Int. Ed.*, 2012, **51**, 11585-11588.
33. H. Gunera, E. Ozgura, G. Kokturkb, M. Celikc, E. Esenb, A. E. Topala, S. Ayasd, Y. Uludagb, C. Elbukena and A. Dana, *Sens. Actuators B Chem.,* 2017, **239**, 571-577.
34. Y. Liu, Q. Liu, S. Chen, F. Cheng, H. Wang and W. Peng, *Sci. Rep.*, 2015, **5**, 12864.
35. G. J. Nusz, A. C. Curry, S. M. Marinakos, A. Wax and A. Chilkoti, *Acs Nano*, 2009, **3**, 795-806.
36. R. Ogier, L. Shao, M. Svedendahl and M. Kall, *Adv. Mater.*, 2016, **28**, 4658-4664.
37. B. Ai, S. Larson, L. Bradley and Y. Zhao, *Adv.Mater.Interfaces*, 2018, **5**, 1800975.
38. Z. Wu, W. Li, M. N. Yogeesh, S. Jung, A. L. Lee, K. McNicholas, A. Briggs, S. R. Bank, M. A. Belkin, D. Akinwande and Y. Zheng, *Adv. Opt. Mater.*, 2016, **4**, 2035-2043.
39. S. Y. Chou, P. R. Krauss and P. J. Renstrom, *Science*, 1996, **272**, 85-87.

View Article Online
DOI: 10.1039/C9NR00455F

40. Y. Zheng, J. Bian, X.-L. Wang, J.-X. Liu, P. Feng, H.-X. Ge, O. J. F. Martin and W.-H. Zhang, *Light-Sci. Appl.*, 2016, **5**, e16156.